Acta Pharmaceutica Sinica B 2023;13(12):5121−5134

Chinese Pharmaceutical Association
Institute of Materia Medica, Chinese Academy of Medical Sciences

Acta Pharmaceutica Sinica B

www.elsevier.com/locate/apsb
www.sciencedirect.com

ORIGINAL ARTICLE

Orange-derived extracellular vesicles nanodrugs for efficient treatment of ovarian cancer assisted by transcytosis effect

Feng Long[a,†], Yao Pan[a,†], Jinheng Li[a,†], Suinan Sha[a], Xiubo Shi[a], Haoyan Guo[a], Chuanqing Huang[a], Qian Xiao[a], Chao Fan[a], Xingmei Zhang[b], Jun-Bing Fan[a,*], Ying Wang[a,*]

[a]*Cancer Research Institute, Experimental Education/Administration Center, Key Laboratory of Functional Proteomics of Guangdong Province, School of Basic Medical Sciences, Southern Medical University, Guangzhou 510515, China*
[b]*Department of Neurobiology, School of Basic Medical Sciences, Southern Medical University, Guangzhou 510515, China*

Received 13 February 2023; received in revised form 4 April 2023; accepted 14 April 2023

KEY WORDS

Extracellular vesicles;
Transcytosis;
Cancer treatment;
Drug delivery system;
Targeted modification;
Receptor-mediated endocytosis;
Intracellular trafficking;
Recycling endosome

Abstract Extracellular vesicles (EVs) have recently received much attention about the application of drug carriers due to their desirable properties such as nano-size, biocompatibility, and high stability. Herein, we demonstrate orange-derived extracellular vesicles (OEV) nanodrugs (DN@OEV) by modifying cRGD-targeted doxorubicin (DOX) nanoparticles (DN) onto the surface of OEV, enabling significantly enhancing tumor accumulation and penetration, thereby efficiently inhibiting the growth of ovarian cancer. The obtained DN@OEV enabled to inducement of greater transcytosis capability in ovarian cancer cells, which presented the average above 10-fold transcytosis effect compared with individual DN. It was found that DN@OEV could trigger receptor-mediated endocytosis to promote early endosome/recycling endosomes pathway for exocytosis and simultaneously reduce degradation in the early endosomes-late endosomes-lysosome pathway, thereby inducing the enhanced transcytosis. In particular, the zombie mouse model bearing orthotopic ovarian cancer further validated DN@OEV presented high accumulation and penetration in tumor tissue by the transcytosis process. Our study indicated the strategy in enhancing transcytosis has significant implications for improving the therapeutic efficacy of the drug delivery system.

*Corresponding authors.
E-mail addresses: fjb2012@mail.ipc.ac.cn (Jun-Bing Fan), ningmengquan@gmail.com (Ying Wang).
†These authors made equal contributions to this work.
Peer review under the responsibility of Chinese Pharmaceutical Association and Institute of Materia Medica, Chinese Academy of Medical Sciences.

https://doi.org/10.1016/j.apsb.2023.04.006

1. Introduction

With the development of targeted drug delivery systems for cancer treatment, nano-technology has contributed substantially to the exploitation of smart carriers in recent decades[1]. However, an extremely complex tumor microenvironment, characterized by abnormal vasculature, high cell density, and dense extracellular matrix, can critically hinder the access of drug delivery systems into the deep tumor tissues resulting in inadequate accumulation and treatment failure[2−5]. Thus, an effective strategy of nanoparticulate drug delivery system to improve deep penetration ability is highly desired in solid tumors. Transcytosis is an important active transport process by which biomacromolecules can be actively transferred from one cell to another cell[6−8]. And transcytosis has been proven as an efficient approach in elevating tumor penetration of nanoparticles for cancer therapy[9−12]. In addition to the enhanced permeability and retention effect (EPR), it has been reported that nanoparticles entered into tumor tissues mainly depend on the active transcytosis effect[13,14]. However, the transcytosis effect of traditional nanoparticles remains limited to causing low accumulation and poor deep penetration ability, resulting in unsatisfied cancer treatment efficacy. Therefore, designing and developing new strategies to improve the transcytosis capacity of nanodrugs is critically needed for efficient drug delivery.

Cell-derived extracellular vesicles (EVs) are acknowledged as crucial entities to regulate the physiological functions of multicellular organisms in an intercellular transmission manner[15−17]. Compared with synthetic nano-carriers, EVs as drug carriers have greater application potential due to their desirable properties such as nano-size, biocompatibility, and high stability[18−21]. In particular, EVs have superior cellular uptake ability and intrinsic transcytosis effect, enabling them to efficiently traverse physiological barriers and penetrate dense tumor tissue[22,23]. Among them, plant-derived EVs showcase cost-efficient production and good safety due to their extensive natural source and defense against zoonotic or human pathogens. We previously developed citrus fruit-derived EV nanodrug presenting great cellular internalization, thus achieving efficient drug delivery and significantly enhancing anti-glioma efficacy assisted by transcytosis[24]. Thus, comprehensively investigating how the EV-based nanodrugs accumulate and deeply penetrate the tumor assisted by transcytosis has significant implications for developing an effective drug delivery system to achieve desirable therapeutic efficacy.

Oranges are among the most widely used natural products in the world and contain abundant bioactive components such as vitamin C, vitamin E, and flavonoid components (hesperidin)[25], which have the potential of reducing the risk of various cancer and improving immunity[26−29]. Thus, orange-derived EV (OEV) served as a carrier candidate representing the great potential for disease treatment. Herein, we demonstrated that the enhanced transcytosis occurred in the interaction between cancer cells and targeted OEV-based drug delivery system to improve tumor penetration ability, resulting in achieving great therapeutic efficacy for ovarian cancer. As a proof of concept, we fabricated a cRGD-targeted OEV-based drug delivery system (DN@OEV), composed of cRGD-targeted doxorubicin (DOX) nanoparticles (DN) patched on the surface of OEV, to investigate their transcytosis process in ovarian cancer cells and validate their therapy efficacy for ovarian cancer. Firstly, amino groups of cRGD linked with carboxyl groups of heparin to prepare heparin-cRGD (HR), and then HR as a carrier conjugated with pH-sensitive adipic acid dihydrazide-DOX (ADH-DOX) to prepare DN. Owing to the abundant cell membrane proteins on the surface of OEV, active amino groups of OEV could readily react with the additional carboxyl groups of heparin in DN. Thus this patching strategy would significantly enhance DOX and cRGD loading efficiency in OEV. In the construction of DN@OEV, cRGD as a targeting ligand had a high affinity with integrin $\alpha_v\beta_3$ overexpressed in ovarian cancer cells, and OEV as carriers enabled to effectively deliver DN to ovarian cancer cells. DN@OEVs were internalized into ovarian cancer cells *via* receptor-mediated endocytosis to promote early endosome/recycling endosomes pathway for exocytosis, and simultaneously reduce early endosomes-late endosomes−lysosome pathway for degradation. Thus, the transcytosis process of cancer cell-DN@OEV interaction involved in endocytosis, intracellular trafficking, and exocytosis was enhanced (Fig. 1).

2. Materials and methods

2.1. Materials

Heparin sodium salt (63007131, Mn = 1.25 kDa, 189 U/mg) was purchased from Sinopharm Chemical Reagent Co. (Shanghai, China). Doxorubicin (DOX, A603456) was purchased from Sangon Biotech (Shanghai, China), and cRGD peptide was synthesized by BAM BIOTECH Co., Ltd. (Xiamen, China). The BCA protein quantification assay kit (KGP903), CD81 (ab109201), calnexin (ab22595), β-actin (ab8227), Ki67 (ab21700), CD34 (ab81289), integrin αv (ab179475), integrin β3 (ab179473), Rab5 (ab302987), Rab7 (ab137029), Rab11 (ab65200) primary antibodies and Alexa Fluor® 488 goat anti-rabbit secondary antibody (ab150081) were purchased from Abcam company (USA). Horseradish peroxidase (HRP)-conjugated anti-rabbit secondary antibody (BS13278) was purchased from Bioworld Technology. Exo1 was purchased from APExBIO. PKH26 dye (PKH26GL) was obtained from Sigma−Aldrich. Hoechst 33342 (C1028) was purchased from Beyotime Biotechnology (Shanghai, China). Sulfo-Cyanine7 NHS ester (R-H-7109) was purchased from Xi'an Ruixi Biological Technology Co., Ltd. (Xi'an, China).

2.2. Isolation and purification of orange-derived EVs

Orange-derived EVs (OEVs) were isolated from orange juice as previously described method[20]. In brief, orange juice was centrifuged using different conditions (500×*g* for 10 min, 2000×*g* for 20 min, 5000×*g* for 30 min, 10,000×*g* for 1 h, and 100,000×*g* for 2 h) by Optima XPN Ultracentrifuge (Beckman Coulter, USA) and the sediments then isolated on a sucrose gradient (8%, 30%,

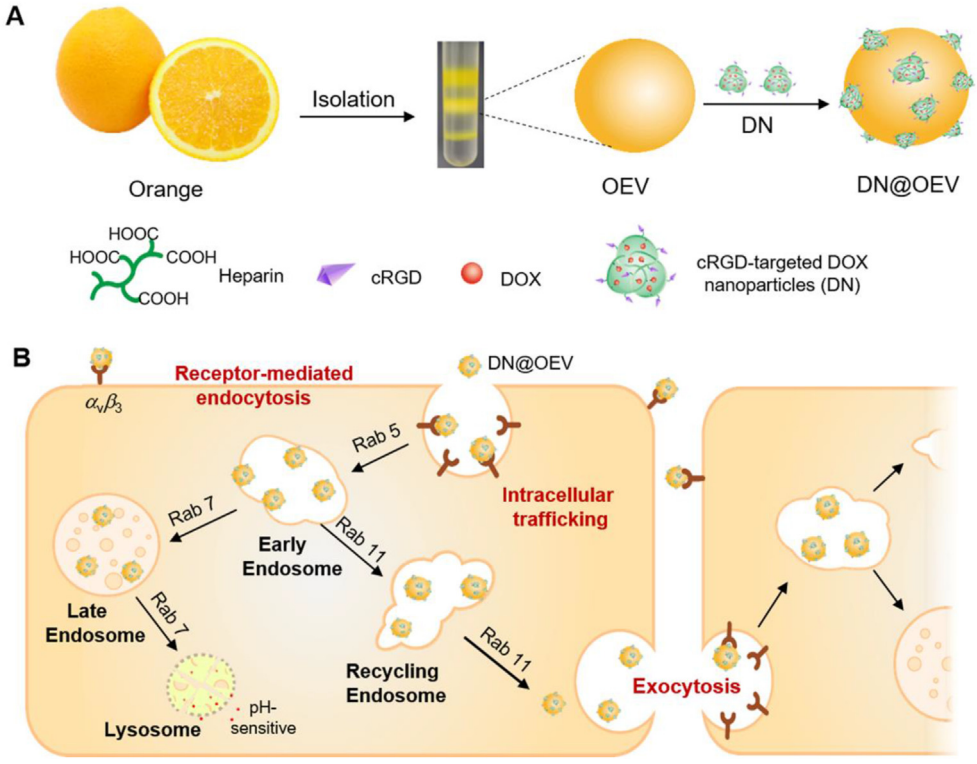

Figure 1 Schematic illustration of the preparation of OEV based nanodrug (DN@OEV) and the transcytosis process of DN@OEV in SKOV3 cells. (A) cRGD-targeted doxorubicin (DOX) nanoparticles (DN) were devised to modify on the surface of OEV thereby preparing DN@OEV; (B) DN@OEV were internalized into SKOV3 cell *via* integrin $\alpha_v\beta_3$-mediated endocytosis, subsequently undergoing early endosomes/recycling endosomes pathway to induce exocytosis and early endosomes/late endosomes to lysosome pathway to degrade. The enhanced transcytosis occurred facilitating targeted-EV based drug delivery system to achieve great therapeutic efficacy for ovarian cancer.

45%, and 60% sucrose in 20 mmol/L Tris−HCl, pH 7.2). The protein concentration of OEV was determined by a BCA protein quantification assay kit. The size distribution and the morphology of the OEVs were measured by dynamic light scattering (DLS) using a Zetasizer Nano-Zs (Malvern Instruments, UK) and Transmission electronic microscopy (TEM) (Hitachi HC-1, 80 kV) after negative staining with phosphotungstic acid, respectively.

2.3. *Preparation and characterization of DN@OEV*

Succinylated-heparin was synthesized as previously described[24]. Succinylated-heparin (50 mg), cRGD peptide (6 mg), 1-ethyl-3,3 dimethylaminopropylcarbodiimide hydrochloride (EDC, 6 mg), and *N*-hydroxysuccinimide (NHS, 6 mg) were mixed and reacted in 2 mL of dimethyl sulfoxide (DMSO) at room temperature for 12 h to prepare heparin-cRGD (HR). Next, the resulting HR product was dialyzed by using a dialysis membrane (MWCO 3500) and then lyophilized. DOX (4 mg) and adipic dihydrazide (ADH, 4 mg) were mixed into 2 mL of methyl alcohol and reacted at room temperature for 12 h using a trace amount of acetic acid as the catalyst. After evaporating the solvent, the crude product ADH-DOX (AD) was obtained. And then, HR (20 mg), the obtained crude AD, and EDC (8 mg) were reacted in deionized water for 6 h at room temperature. After that, the obtained product solution was adjusted to the pH value of 10 and dialyzed in deionized water for 48 h to prepare pure HR-AD (DN). Cy7-labeled DN (Cy7-DN) was synthesized as follows: succinylated-heparin (50 mg), 100 μg Cy7-amine, EDC (8 mg), and NHS (8 mg) were dissolved in 2 mL DMSO and reacted for 3 h at room temperature, and then 6 mg cRGD was added and reacted for another 12 h. After that, the reaction product was dialyzed using a dialysis membrane (MWCO 3500) for 48 h and lyophilized to obtain Cy7-labeled HR (Cy7-HR). The preparation method of Cy7-DN was similar to that of DN using Cy7-HR as raw materials. The preparation of Cy7-DN@OEV was similar to DN@OEV using Cy7-DN as raw materials. The amount of Cy7 in DNs was measured by a UV−Vis spectrometer at 750 nm. It detected 0.3 μg Cy7 in 1 μg of OEV, and 0.015 μg Cy7 in 1 μg of DN.

DN@OEV was prepared as previously described[24]. 100 μg of OEV and 1000 μg of DN were reacted in deionized water at room temperature for 12 h by using EDC (6 mg) and NHS (6 mg) as catalysts, respectively. The obtained product DN@OEV was washed twice with PBS and then ultracentrifuged at 120,000×*g* for 1 h, and re-dispersed in PBS buffer. For the preparation of cRGD-OEV, 100 μg of OEV and HR (equivalent amount of HR in 1000 μg DN) were reacted in deionized water at room temperature for 12 h by using EDC (6 mg) and NHS (6 mg) as catalysts, respectively. The obtained product cRGD-OEV was washed twice with PBS and then ultracentrifuged at 120,000×*g* for 1 h, and re-dispersed in PBS buffer. PKH26-labeled OEV and PKH26-labeled cRGD-OEV were prepared according to the standard procedures of manufacturers. Directly confirmed the structure of DN came from ^{1}H NMR spectra (Bruker Biospin, AVANCE III HD 600 MHz). The amount of cRGD peptide in DN was measured by

BCA assay and the DOX concentration was determined by a UV−Vis spectrometer at 480 nm. UV spectra detected DOX content in DN@OEV to deduce cRGD content in DN@OEV according to cRGD content in DN. BCA assay was used to detect cRGD peptide in unreacted HR and determine the cRGD amount in cRGD-OEV. The loading efficiency of DOX and cRGD in DN or DN@OEV was calculated by Eq. (1):

$$\textit{Loading efficiency}\ (\%) = (\textit{Weight of agent in samples}/\textit{Initial weight of agent}) \times 100 \quad (1)$$

The size distribution and morphology of the DN and DN@OEV were measured by DLS and TEM after negative staining with phosphotungstic acid.

2.4. Cell culture

The human ovarian cancer cell line SKOV3 and mouse breast cancer cell line 4T-1 were purchased from the Cell Resource Center of the Chinese Academy of Science (Shanghai, China). The SKOV3-Luc cells were generated in our laboratory *via* transfection with a reporter gene encoding firefly luciferase. SKOV3 and 4T-1 cells were cultured in RPMI-1640 medium, supplemented with 10% FBS (Gibco, USA) and 1% penicillin−streptomycin (Gibco, USA). All cells were maintained in a humidified incubator with 5% CO_2 at 37 °C.

2.5. Cellular uptake assay

SKOV3 and 4T-1 cells were seeded in 6-well plates at a density of 3×10^6 cells/well and incubated for 12 h. Then PKH26-labeled OEV and PKH26-labeled cRGD-OEV (with EVs concentration 2 μg/mL), free DOX, DN, and DN@OEV (with DOX concentration 2.5 μg/mL) were added to the well, and incubated for 4 h at 37 °C, respectively. After incubation, cells were washed with PBS, centrifuged, and re-suspended in PBS solution for detecting DOX or PKH26 signal (PE channel) by flow cytometry (Becton Dickinson, USA). The results were analyzed using FlowJo 7.6 software.

2.6. Transcytosis effect detected by flow cytometry

SKOV3 and 4T-1 cells were seeded in 6-well plates at a density of 3×10^6 cells/well and incubated for 12 h, respectively. PKH26-OEV and PKH26-cRGD-OEV, free DOX, DN, and DN@OEV were respectively added to the well and co-incubated with SKOV3 cells or 4T-1 cells for 4 h at 37 °C. After replacing the culture medium, new SKOV3 cells or 4T-1 cells stained by Hochest3342 for 10 min at room temperature were added to the wells for co-incubation with different time points (4, 12, 16, and 24 h). After that, cells were washed with PBS, centrifuged, and re-suspended in PBS solution for detecting dual-fluorescent channels (PE/PKH-26 or DOX and V450/Hochest33342) by flow cytometry.

2.7. Transcytosis effect detected by laser scanning confocal microscope

To conduct a transcytosis assay experiment, Transwell polyester membranes (Corning, NY, USA) with pore sizes of 0.4 μm on 24-well were used. The same amount of SKOV3 cells or 4T-1 cells (2.5×10^4 cells) were respectively added to the upper chamber and bottom chamber, and SKOV3 cells or 4T-1 cells in two chambers were individually incubated for 24 h. And then PKH26-OEV or PKH26-cRGD-OEV were added to the upper chamber and incubated with cells for 4 h. After that, the medium in the upper compartment was replaced by the fresh one. The Upper chambers were then put in the bottom chamber containing SKOV3 cells or 4T-1 cells, and they co-incubated for the extra 12 h. And then, the cell culture medium was discarded and the Transwell polyester membranes seeded with cells in the bottom chamber were washed with PBS 3 times, and then fixed with 4% paraformaldehyde (PFA) for 10 min, and stained with Hoechst 33342. The transcytosis in different groups was imaged using a laser scanning confocal microscope (LSCM, Nikon, Japan).

2.8. Penetration ability assay of DN@OEV in LN229 multicellular spheroids (MCSs)

The MCSs were cultured according to the previously described method[30]. Briefly, a culture dish (Corning, NY, USA) was covered by 5 mL of hot agarose (2%, *w/v*) solution and then cooled at room temperature. Then human glioma LN229 cells were cultured at a density of 2×10^6 cells in each culture dish with 6 mL DMEM medium. The MCSs formed after incubation for 7 days and were isolated for use. MCSs with appropriate size (200−300 μm) were collected and incubated with different samples in 96-well plates in DMEM medium and pretreated by Exo1 (10 μg/mL) for 12 h or not. After incubating for 6 h, the MCSs were washed with PBS (pH 7.4) three times and observed with an LSCM imaging system in PBS (pH 6.7).

2.9. Immunofluorescence detection

SKOV3 cells were cultured on the chamber slide with a density of 2×10^4 cells/well at 37 °C for 24 h. Then the medium was replaced by fresh medium containing PKH26-OEV and PKH26-cRGD-OEV (2 μg/mL EVs) and co-incubated at 37 °C for 4 h. After that, cells were fixed with 4% PFA for 10 min at room temperature and washed with PBS twice. The cells were then permeabilized using 0.25% Triton X-100 in PBS for 15 min and blocked for 30 min using 1% BSA at room temperature. After blocking, cells were incubated with Rab 5, 7, or 11 antibodies overnight at 4 °C. Unbounded antibodies were removed by washing with PBS twice. Cells were then incubated with Alexa Fluor® 488 goat anti-rabbit secondary antibody at room temperature for 1 h, and washed with PBS twice. Then cells were stained with Hoechst33342 for 5 min and washed three times with PBS. The samples were observed by LSCM.

2.10. Establishment of the nude mice bearing orthotopic ovarian cancer

All procedures for animal use were approved by the Institutional Animal Care and Use Committee (IACUC) at Southern Medical University, Guangzhou, China. Female BALB/c nude mice (15−20 g) were purchased from Guangdong Medical Laboratory Animal Center. The nude mice were anesthetized *via* intraperitoneal injection with 1% sodium pentobarbital (8 μL/g). The anesthetized animals were placed in a prone position and fixed on an operating table. An approximately 1 cm of incision was made vertically near the spine between the right costal arch and the

femur. The abdominal cavity was opened according to an anatomical level to expose the ipsilateral ovary and the fallopian tube. The ovary was carefully fixed using ophthalmic forceps, and the prepared SKOV3-Luc cells suspension (10 μL, 4×10^4 cells/μL) was gradually injected into the ovary. After verifying the absence of active bleeding, we carefully put the ovary back into the abdominal cavity and sutured the incision. Mice were fed in an SPF environment after surgery, and tumor growth was monitored using an *in vivo* imaging system (IVIS Lumina II, Caliper, USA).

2.11. *In vivo biodistribution and tumor targeting ability detection*

The orthotopic SKOV3-Luc ovarian cancer xenograft nude mouse model ($n = 3$) was intraperitoneally injected with free Cy7, Cy7-DN, and Cy7-DN@OEV. At 0.5, 6, 12, 24, 48, and 96 h after administration, the mice with the Cy7 fluorescence and luciferase signal (96 h) imagings were observed by IVIS. The mice were sacrificed at 96 h and the ovarian primary tumors and major organs (heart, liver, spleen, lung, and kidney) were harvested and visualized by IVIS.

The orthotopic SKOV3-Luc ovarian cancer xenograft nude mouse model ($n = 3$) was intraperitoneally injected with DOX, DN, and DN@OEV. After 24 h post-injection, the mice were sacrificed to collect the tumors. The tumor tissues of each group were fixed in 4% PFA for 24 h, embedded in paraffin wax, cut into 4 μm-thick sections, and stained with Hoechst33342 for 5 min. After washing with PBS, the sections were observed by LSCM to detect their targeting capability.

2.12. *Zombie fixation and nanoparticle circulation*

Zombie experiments were conducted as the previous method[13]. The nude mice bearing orthotopic ovarian cancer were established. A zombie mouse model bearing orthotopic ovarian cancer was developed by fixing the whole mouse using transcardiac perfusion with 4% PFA for 30 min at 37 °C. And then the fixed animal was placed inside another box for 1 h of further fixation. After that, the fixative was removed and DOX, DN, and DN@OEV solution (DOX concentration of 2.5 mg/kg in 10% FBS solution) were added for circulation by intravenous injection using a peristaltic pump (BT100L-CE, China). The circulation lasted for 4 h for samples using a 5 min/mL of flow rate. The concentration of samples was the same as that in the live animal by intraperitoneal injection. The tumors were then resected from these mice to detect DOX concentration using a cell imaging multi-mode reader (BioTek Cytation 5, USA).

2.13. *The immunogenicity evaluation*

To evaluate the acute immune responses induced by our nanodrug *in vivo*, we assessed the concentration of IL-6, IL-1β, IP-10, and TNF-α in C57BL/6 immuno-intact mice (6−8 weeks) after intraperitoneal administration of different samples. Briefly, the C57BL/6 mice were divided into five groups ($n = 3$) and injected with DOX, DN, DN@OEV (3 mg/kg DOX), and OEV (10 mg/kg EV equivalently to DN@OEV) using PBS as control. After administration for 24 h, C57BL/6 mice were sacrificed to get the serum, and then cytokines including IL-6, IL-1β, IP-10, and TNF-α, were analyzed in the serum using ELISA kits according to the manufacturer's instruction (Mlbio, China).

2.14. *In vivo antitumor efficacy*

Three days after building an orthotopic ovarian cancer-bearing nude mouse model, the tumors were monitored by IVIS luminescent imaging. Consequently, the nude mouse models were randomly divided into four different groups ($n = 5$), and then the mice were intraperitoneally injected into PBS, free DOX, DN, or DN@OEV (2.5 mg/kg DOX) every three days. The body weight and tumor size were detected every 4 days. After 16 days of treatment, mice were sacrificed and then the primary tumors and major organs (heart, liver, spleen, lung, kidney, and intestine) were excised and observed by IVIS luminescent imaging. The weights and volumes of primary tumors were analyzed. Tumor volume was calculated as Eq. (2):

$$V = \text{Larger diameter} \times (\text{Smaller diameter})^2/2 \quad (2)$$

2.15. *Statistical analysis*

All data were reported as mean ± standard deviation (SD). One-way ANOVA or unpaired two-tailed Student's *t*-tests were used to establish statistical significance using IBM SPSS 19.0 software. Differences were considered significance at $^*P < 0.05$, $^{**}P < 0.01$, $^{***}P < 0.001$.

3. Results and discussion

Based on bioactive ingredients containing the parent plant, we detected 1 μg (protein amount) OEV contained 0.14% vitamin C, 0.12% vitamin E, and 4.06% hesperidin determined by the HPLC method (Supporting Information Fig. S1). It indicated OEV contained abundant bioactive compounds beneficial for medical application as their parent plant. cRGD peptide modified with heparin (HR) conjugated with pH-sensitive ADH-DOX conjugation (AD) to fabricate cRGD-targeted DOX nanoparticles (DN). The additional carboxyl groups of heparin in DN were further conjugated with amino groups of OEV to prepare DN@OEV by amidation reaction. Direct confirmation of the DN structure came from the ^{1}H NMR spectra (Supporting Information Fig. S2). TEM results showed that DN exhibited a small spherical shape and OEV displayed obvious lipid layers. Also, it was observed small particles adhered to the surface of OEV, indicating DN was successfully patched on the surface of OEV (Fig. 2A). The results of DLS showed that the size of the DN and OEV was about 54.9 ± 5.3 nm and 101.4 ± 5.5 nm, and the size of DN@OEV (200.7 ± 9.3 nm) was larger than that of DN and OEV (Fig. 2B). In addition, we detected OEV were enriched in EV' protein markers (CD81 and CD9) while were lack of endoplasmic reticulum marker (Calnexin) determined by the Western blotting, and DN@OEV had the same markers (Fig. 2C). It indicated the prepared DN@OEV had similar bio-function as OEV. UV spectra showed that DN@OEV exhibited similar characteristic absorption peaks at 489 nm, as free DOX (Supporting Information Fig. S3). Also, the weight percentages of cRGD and DOX in the DN were approximately 4.1% and 12.3%, and 1 μg (protein amount) of OEV contained 0.43 μg of cRGD and 4.1 μg of DOX, which were determined by BCA method and UV spectra, respectively (Supporting Information Table S1−S3). Accumulating documents showed that EVs had good stability in physiological condition[18−21]. We also found that OEV and DN@OEV kept stability

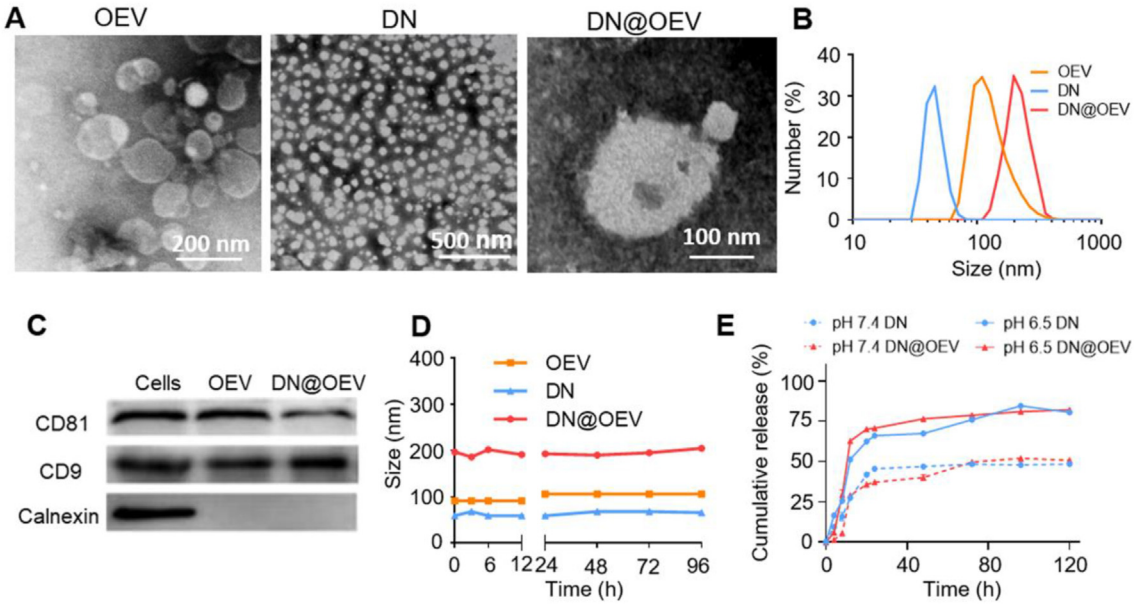

Figure 2 Characterization of OEV, DN and DN@OEV. (A) TEM images of OEV, DN and DN@OEV. (B) The size distribution of DN, OEV, and DN@OEV determined by DLS. (C) The expression of CD81, CD9, and calnexin of OEV and DN@OEV as measured by Western blotting using SKOV3 lysates as a control. (D) The stability of DN, OEV, and DN@OEV in 10% FBS determined by DLS. (E) The release curve of DN and DN@OEV in PBS solution with pH 7.4 and pH 6.5 determined by UV spectrum. The data are shown as mean ± SD ($n = 3$).

within 96 h under 10% fetal bovine serum (FBS) solution (Fig. 2D and Supporting Information Fig. S4). Due to the pH-sensitive properties of DN, we found that DN@OEV could speed up the release of DOX in PBS with pH 6.5 solution while there was no obvious difference between DN and DN@OEV, indicating DN@OEV possessed tumor microenvironment response (Fig. 2E).

We detected ovarian cancer cells (SKOV3) had high expression of $\alpha_v\beta_3$ while breast cancer cells (4T-1) had slightly low expression of $\alpha_v\beta_3$ determined by western blotting (Supporting Information Fig. S5). Thus, we selected SKOV3 cells and 4T-1 cells to compare the biological activities of DN@OEV *in vitro*. We first investigated the cellular internalization ability of PKH26-labeled OEV (PKH26-OEV), PKH26-labeled cRGD-modified OEV (PKH26-cRGD-OEV), DOX, DN, and DN@OEV in both cells (Fig. 3A and Supporting Information Fig. S6). The results of flow cytometry showed that cRGD-OEV presented better cellular uptake ability than OEV in SKOV3 cells ($P < 0.001$), while there was a reduced difference between OEV and cRGD-OEV in 4T-1 cells ($P < 0.05$), indicating targeting effect could enhance the cellular uptake of cRGD-OEV. It was found the cellular uptake ability of DN was higher than that of free DOX in SKOV3 cells, while DN@OEV had the best cellular uptake ability in both cells. It was explained that OEV contained abundant intracellular transporters (162 proteins associated with the transport Gene Ontology term) beneficial to their transport in cells[31]. Thus the introduction of EV could enhance the delivery efficiency of synthetic nanoparticles. Due to OEV being rich in transporter proteins, we conducted Transwell experiments to detect the transcytosis effect of OEV and cRGD-OEV in both cells. In brief, after the sample was co-incubated with cancer cells in the top chamber for 4 h, the medium was replaced and cancer cells in the top chamber continued to co-incubate with cancer cells in the bottom chamber for 12 h. Cancer cells in the bottom chamber were observed by LSCM (Fig. 3B). Compared with PKH26-OEV, PKH26-cRGD-OEV presented enhanced fluorescent intensity in SKOV3 cells (Fig. 3C), while it had a little bit of difference in 4T-1 cells (Fig. 3D), suggesting targeted modification could largely enhance the transcytosis ability of cRGD-OEV. Furthermore, we quantified the transcytosis efficiency of PKH26-OEV and PKH26-cRGD-OEV in both cells by double fluorescence channels (PE and V450) of flow cytometry. Briefly, the sample was co-incubated with cancer cells for 4 h, and then replaced with the medium. After that, cells labeled with Hochest33342 were added and continued to co-incubate for an additional 4 h (Supporting Information Fig. S7). Flow cytometry analyzed cells with PE^+V450^+ were gated to their transcytosis efficiency. It was found that cRGD-OEV could trigger transcytosis in 15.2% of SKOV3 cells, while OEV induced 3.73% of SKOV3 cells to transport. And there were similar results in 4T-1 cells. It indicated that targeting modification could promote the transcytosis process for OEV (Fig. 3E).

Similarly, we detected the transcytosis efficiency of DOX, DN, and DN@OEV using flow cytometry. After co-incubated with cells labeled Hochest33342 for 4 h, it detected DN@OEV could induce transcytosis in 15.8% of SKOV3 cells and 12.7% of 4T-1 cells, while DOX and DN hardly produced transcytosis process (Fig. 4A). It suggested that the introduction of OEV could significantly enhance the transcytosis effect beneficial them to improve the penetration ability in tumor tissue. Furthermore, it was observed that DN@OEV could induce the transcytosis process in more cells as incubation time increased, and they obtained maximum at 16 and 12 h in SKOV3 and 4T-1 cells, respectively. In particular, DN@OEV presented an average above 10-fold transcytosis effect compared with DN. Also, DN@OEV could induce a greater transcytosis effect in SKOV3 cells than in 4T-1 cells, indicating targeting modification could improve the transport capability of EV in specific cancer cells. However, flow cytometry showed that free DOX and DN hardly enhanced transcytosis ability as the incubation time increased, suggesting small molecule drug and synthetic traditional nanoparticles had

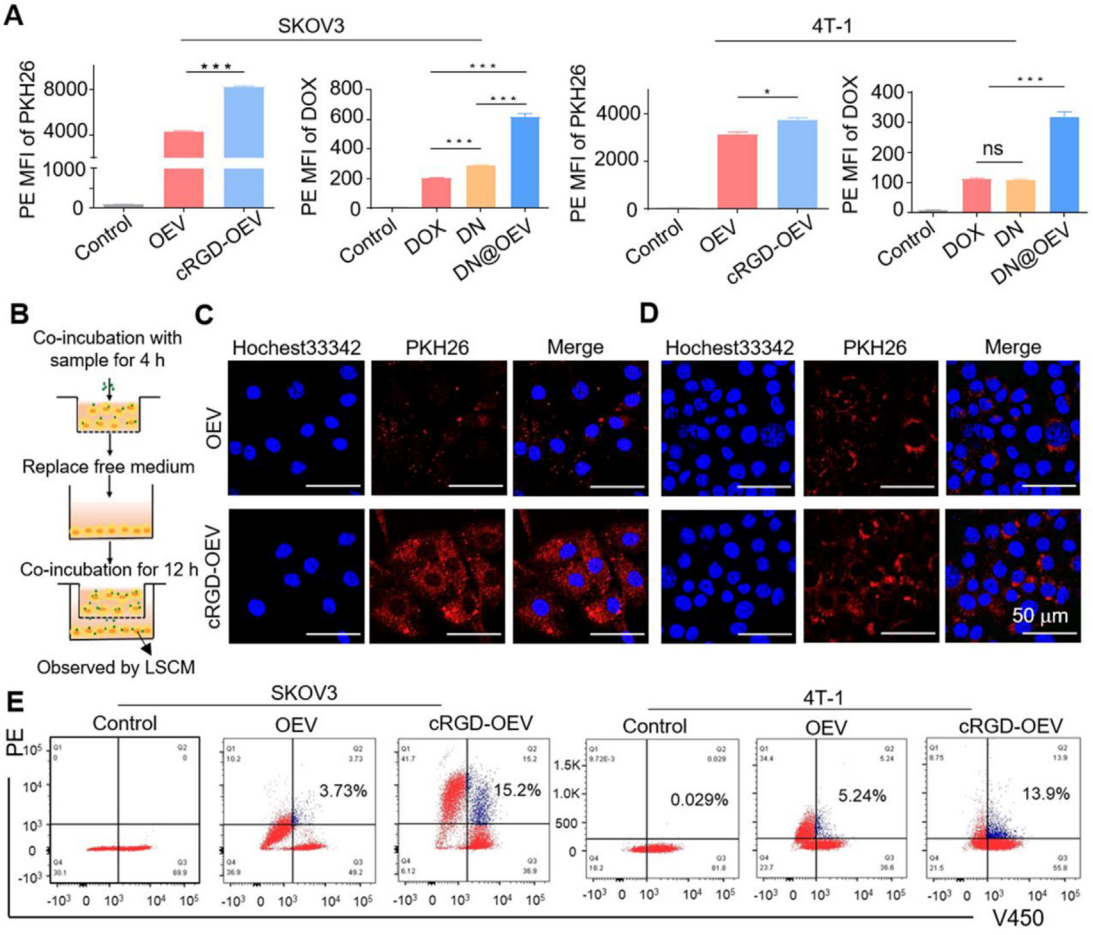

Figure 3 The cellular uptake and transcytosis effect of cRGD-OEV and DN@OEV in SKOV3 and 4T-1 cells. (A) The cellular uptake of PKH26-OEV and PKH26-cRGD-OEV, DOX, DN, DN@OEV in SKOV3 and 4T-1 cells for 4 h, as detected by flow cytometry. The data are shown as mean ± SD ($n = 3$). *$P < 0.05$, ***$P < 0.001$. *ns*, not significant. (B) Protocol of Transwell experiment to verify the transcytosis of PKH26-OEV and PKH26-cRGD-OEV. LSCM images of transcytosis effect of PKH26-OEV and PKH26-cRGD-OEV in (C) SKOV3 and (D) 4T-1 cells at bottom chamber. Scale bar: 50 μm. (E) Quantitative analysis of transcytosis effect of PKH26-OEV and PKH26-cRGD-OEV, in which sample co-incubated with SKOV3 and 4T-1 cells for 4 h and then added cell-labeled Hochest33342 to wells for incubation with 4 h by flow cytometry.

poor transport ability resulting in unsatisfied treatment efficacy (Fig. 4B and C and Supporting Information Fig. S8).

It was reported that glioma LN229 cells had high expression of integrin $\alpha_v\beta_3$[24], and also LN229 cells could be constructed multicellular spheroids (MCSs). Thus, we adopted MCSs of LN229 cells, an *in vitro* three-dimensional (3D) mimicking tumor tissue, to evaluate their penetration ability. To validate whether the paracellular diffusion through transcytosis caused the penetration of PKH26-cRGD-OEV in the MCSs, we also pretreated the MCSs with the exocytosis inhibitor Exo1. It was found that cRGD-OEV had greater penetration ability than OEV. And the pretreatment of Exo1 significantly decreased the cRGD-OEV penetrating ability to the spheroids, indicating the penetration of cRGD-OEV was mainly dependent on the transcytosis effect (Supporting Information Fig. S9). Similarly, we found DN@OEV had the best capability to penetrate the MCSs while DOX and DN had no obvious difference, confirming transcytosis effect of DN@OEV attributed to the OEV effect (Fig. 4D). We detected their cytotoxicity in SKOV3 and 4T-1 cells for 48 h using MTT assay (Fig. 4E and Supporting Information Table S4). It showed that DN@OEV presented the best cytotoxicity in both cells while DOX and DN had similar cytotoxicity, indicating the killing ability of DN@OEV in SKOV3 was enhanced after the introduction of OEV to DN, which was consistent with the results of cellular uptake. Also, it was found that OEV almost had no cytotoxicity in both cancer cells (Supporting Information Fig. S10).

Accumulating documents revealed transcytosis could be initiated by specific receptors or membrane electrostatic absorption and mediated by recycling endosomes[30,32,33]. Receptor-mediated endocytosis was based on specific ligand/receptor interaction and some of the metabolic receptors could be recycled back to the plasma membrane from early endosome, thus inducing transcytosis[34,35]. Regarding the internalization of nanoparticles, nanoparticles first clustered into coated pits and were endocytosed to early sorting endosomes, and then they were selectively transported to late endosomes with a fate of lysosomal degradation or were transferred to recycling endosomes for the destination of the surface in cells by transcytosis[36,37]. Notably, EV underwent a similar intracellular trafficking route and finally could be released outside the cells by recycling endosomes during the generation of EV[38−40]. Thus it was necessary to investigate intracellular

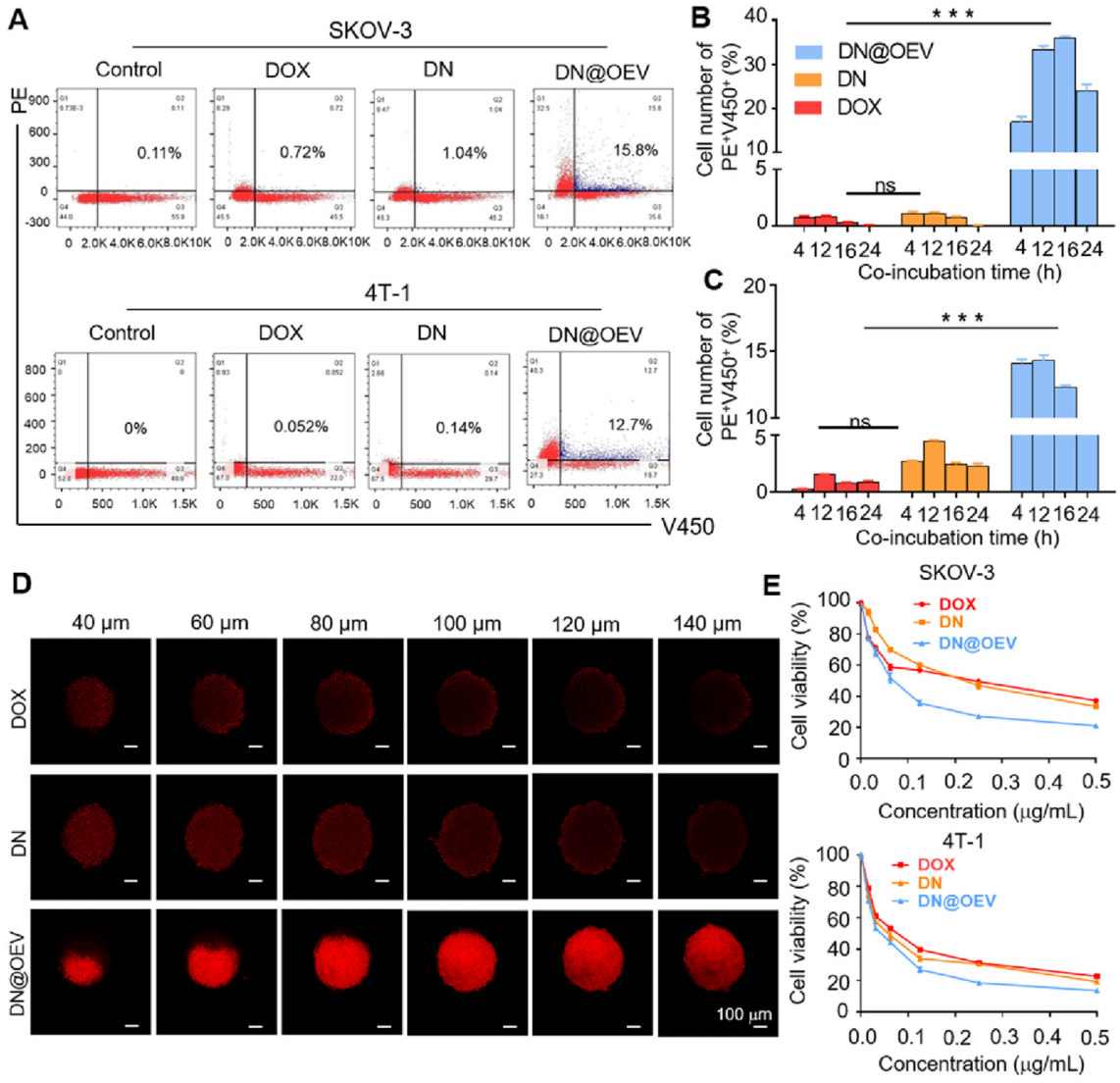

Figure 4 Quantitative analysis of transcytosis effect induced by DOX, DN and DN@OEV by flow cytometry and their cytotoxicity in SKOV3 and 4T-1 cells for 48 h. (A) Flow cytometry detection of transcytosis efficiency of DOX, DN and DN@OEV co-incubated with SKOV3 and 4T-1 cells for 4 h and then added Hochest33342-labeled SKOV3 and Hochest33342-labeled 4T-1 to wells for incubation with 4 h. Quantitative analysis of transcytosis efficiency of DOX, DN and DN@OEV co-incubated with SKOV3 and 4T-1 cells for 4 h and then added (B) Hochest33342-labeled SKOV3 and (C) Hochest33342-labeled 4T-1 to wells for incubation with different time. Mean ± SD ($n = 3$). ***$P < 0.001$; *ns*, not significant. (D) LSCM observation of the penetration ability of DOX, DN and DN@OEV in LN229 MCSs (Scale bar: 100 μm). (E) The cytotoxicity of DOX, DN and DN@OEV in SKOV3 and 4T-1 cells using MTT assay. The data are shown as mean ± SD ($n = 3$).

trafficking to verify the transcytosis process of DN@OEV. Owing to DOX as a DNA intercalator in nuclei[41], it could not observe the whole process of DN@OEV in the cytoplasm. Accordingly, we investigated the intracellular trafficking of OEV and cRGD-OEV in SKOV3 to deduce the transcytosis process of DN@OEV. The intracellular trafficking of EV was controlled by the transporter proteins, such as the involvement of the Rab family in the regulation of membrane trafficking. Thus, we used Rab 5, 7, and 11 to trace early endosomes, late endosomes, and recycling endosomes by immunofluorescence method, respectively[42]. Meanwhile, LysoTracker-green was employed to label lysosomes. The co-localization of PKH26-OEV and PKH26-cRGD-OEV with these endosomes was observed by LSCM and analyzed by ImageJ software (Fig. 5A). Compared to the intracellular trafficking pathway OEV, cRGD-OEV had the increased colocalization in early endosomes (Rab 5) and recycling endosomes (Rab 11) and the decreased colocalization in late endosomes (Rab 7) and lysosomes (LysoTracker), indicating receptor-mediated endocytosis for cRGD-OEV was beneficial to increase exocytosis effect by early endosome/recycling endosomes pathway and decrease their lysosomal degradation (Fig. 5B). Thus, the similar transcytosis initiated by DN@OEV was: after DN@OEV were internalized to the early endosome, part of them were selectively transported to late endosomes and fused with lysosome for degradation; on the other hand, more of DN@OEV in early endosome were transferred to recycling endosomes for exocytosis. It suggested transcytosis capability of DN@OEV could be significantly enhanced by receptor−ligand interaction to promote their accumulation and penetration in tumor tissues, thereby presenting anticipated antitumor ability.

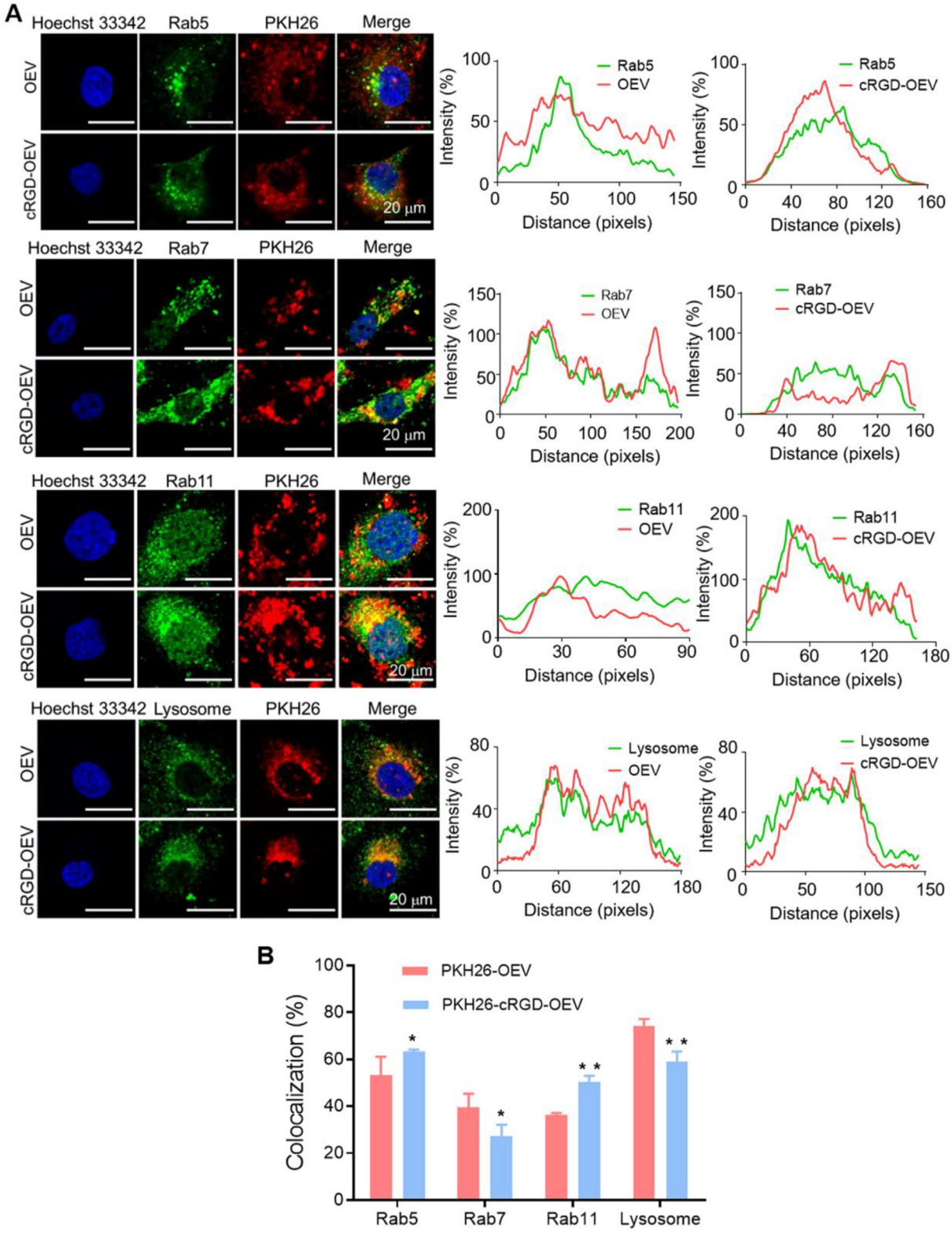

Figure 5 The intracellular trafficking route induced by PKH26-OEV and PKH26-cRGD-OEV in SKOV3 cells. (A) The intracellular trafficking pathway of PKH26-OEV and PKH26-cRGD-OEV co-localization of Rab 5, 7 and 11 and LysoTracker staining. Scale bar: 20 μm. (B) The co-localization efficiency of PKH26-OEV and PKH26-cRGD-OEV with Rab 5, 7 and 11 and Lysosome based on (A) results. The data are shown as mean ± SD ($n = 3$). *$P < 0.05$, **$P < 0.01$.

Based on the *in vitro* biological properties of DN@OEV, we established the orthotopic SKOV3-Luc ovarian cancer xenograft nude mouse model to conduct *in vivo* experiments. The *in vivo* biodistribution and cancer targeting capacity of Cy7 labeled-DN (Cy7-DN) and Cy7 labeled-DN@OEV (Cy7-DN@OEV) were investigated in the mouse model *via* intraperitoneal injection. Real-time images of biodistributions of free Cy7, Cy7-DN, and Cy7-DN@OEV were observed at different times after administration, through which the tumor was monitored by the bioluminescence of Luc-SKOV3 cells. The results show that the fluorescent intensity of Cy7-DN@OEV was higher than that of free Cy7 and Cy7-DN at 96 h after administration (Fig. 6A). Mice were sacrificed at 96 h after injection and the excised organs (heart, liver, spleen, lung, kidney, and tumor) were carefully compared the fluorescence accumulation. It showed that Cy7-DN@OEV were mainly distributed in the liver, spleen, kidney, and tumor, and their accumulation at the tumor site was much higher than Cy7-DN, suggesting that DN@OEV had the good cancer-targeting ability (Fig. 6B). Furthermore, we tested the accumulation of DOX, DN, and DN@OEV in tumor tissues of orthotopic SKOV3-Luc ovarian cancer xenograft nude mouse model by LSCM (Fig. 6C and Supporting Information Fig. S11). It was detected that a large number of DN@OEV accumulated in tumor tissues compared with free DOX and DN, indicating DN@OEV exhibited good tumor accumulation and penetration ability.

Chan and his co-workers[13] adopted the zombie mouse model, in which tumor-bearing mice were perfused with PFA to deactivate any cellular activity, to roughly verify the effect of active trans-endothelial transport of nanoparticles. Similarly, we developed a zombie mouse model with orthotopic ovarian cancer and the fixation step would almost block the morphological changes underlying trans-endothelial transport (Supporting Information Video S1). Thus it would roughly investigate the influence of transcytosis ability on the accumulation of DN@OEV in the zombie mouse model by intravenous circulation. We simultaneously compared the accumulation of DN@OEV in ovarian cancer-bearing live mouse model by intraperitoneal injection (Fig. 6D). Compared to the results in the tumor-bearing live mouse, DN@OEV accumulation was largely decreased after blocking trans-endothelial transport in the zombie mouse model. It indicated the transcytosis effect played a dominant role in the tumor accumulation of EV-based nanodrug though there were possibly other transport pathways, such as the EPR effect. In addition, DN accumulation was significantly lower than DN@OEV accumulation in tumor-bearing live mice, confirming synthetic nanoparticles presented poor transcytosis ability. Interestingly, DN accumulation in tumor-bearing mice was lower than

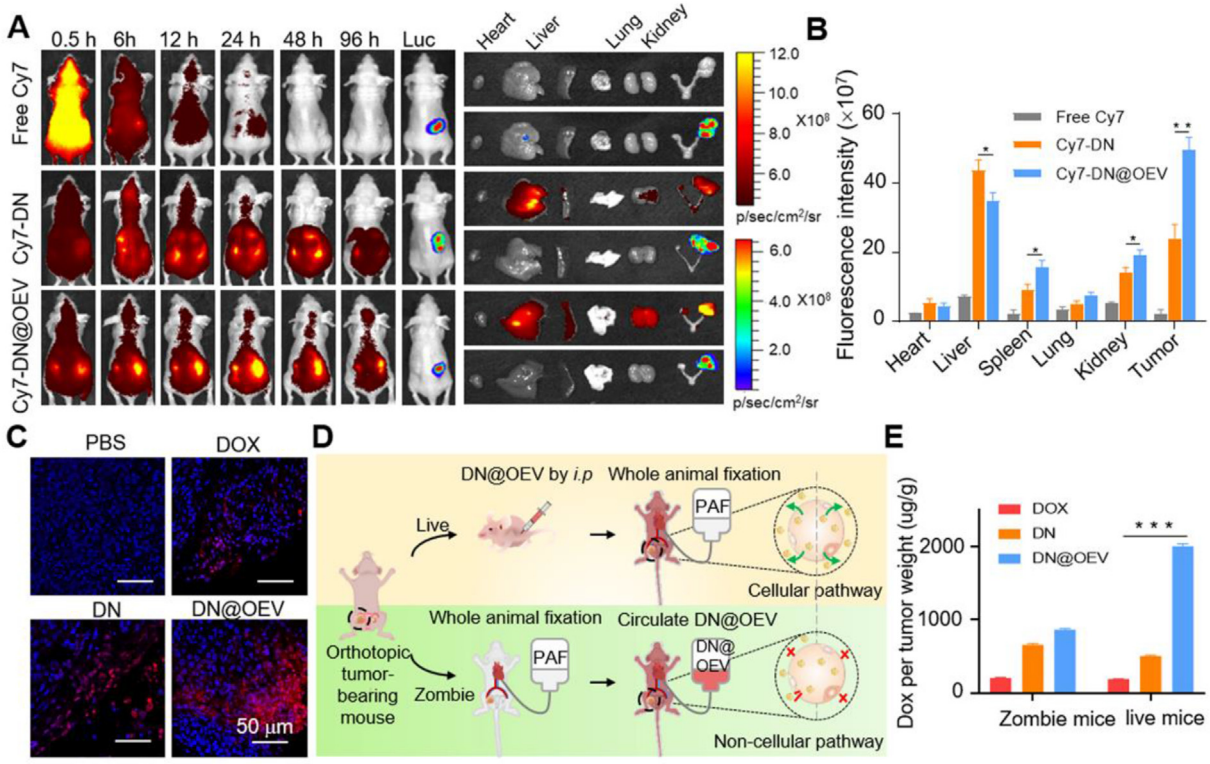

Figure 6 *In vivo* biodistribution and cancer targeting ability of DN@OEV in orthotopic SKOV3-Luc bearing ovarian cancer nude mouse. (A) *In vivo* fluorescence images of orthotopic SKOV3-Luc bearing ovarian cancer nude mouse at different time points after intraperitoneal injection of free Cy7, Cy7-DN and Cy7-DN@OEV. After 96 h, mice were sacrificed and their major organs and tumors were collected to detect Cy7 and Luc signals. (B) The corresponding semiquantitative results of *ex vivo* organs and tumors in different groups. (C) Confocal images of the tumor tissues in orthotopic ovarian cancer mouse after intraperitoneal injection of PBS, DOX, DN and DN@OEV. Scale bar: 50 μm. (D) Protocol of Zombie mouse and live mouse to verify the transcytosis effect DN@OEV *in vivo*. After development of Zombie mouse bearing orthotopic ovarian cancer, mouse was first fixed by PFA and circulated with DN@OEV. (E) DOX, DN and DN@OEV accumulation in tumor tissues of Zombie mouse and live mouse. Results are represented as mean ± SD ($n = 3$). *$P < 0.05$, **$P < 0.01$ and ***$P < 0.001$.

that in Zombie mouse model (Fig. 6E). It was possibly attributed to different administration routes and complex metabolic processes in live mice, such as the reticuloendothelial system in blood and metabolic organs. Although there were different administration routes between the zombie mouse experiment and the live mouse model for DN@OEV, our zombie mouse model results still disclosed that active transcytosis would unlock strategies to enhance the delivery efficiency of EV-based nanodrug in tumor therapy.

The antitumor efficacy of DN@OEV on orthotopic SKOV3-Luc ovarian cancer xenograft nude mouse model was subsequently evaluated. The tumor growth was measured by monitoring luminescence intensity *via in vivo* imaging system (IVIS). All mice were injected SKOV3-Luc cells into the ovaries, followed by treatment and measurement of bioluminescence after 3 days (Day 0). The results show that compared to free DOX and DN, significant suppression of tumor growth was observed in mice treated with DN@OEV. Simultaneously, we monitored body weight in all groups to estimate their potential adverse effects. It showed the body weight of mice in DN@OEV and PBS groups remained stable during the process of the treatment period, while the DOX group and DN group exhibited decreased body weight in the late period of treatment. The results indicate that DN@OEV possessed good biosafety compared with free DOX and DN (Fig. 7A–C). After 16 days of treatment, mice were sacrificed and the tumors were excised for further evaluation (Fig. 8A). The average primary tumor weight and volume treated by DN@OEV (weight, 48.57 ± 71.88 mg; volume, 50.09 ± 132.06 mm^3) were significantly smaller than those of PBS (weight, 1190.25 ± 295.00 mg; volume, 1566.25 ± 356.38 mm^3), DOX (weight, 400.72 ± 223.04 mg; volume, 397.88 ± 258.33 mm^3) and DN (weight, 195.87 ± 97.01 mg, volume, 240.08 ± 113.92 mm^3) (Fig. 8B).

The luminescence intensity showed that DN@OEV exhibited a more significant antitumor effect than DOX and DN. Moreover, it was observed visible metastatic nodules could be detected in the intestines of the PBS group (Fig. 9A). In addition, H&E staining of the main organs showed that there was no obvious tissue damage except for the metastases nodules in the intestines of the PBS (Fig. 9B and Supporting Information Fig. S12). Also, we detected DN@OEV induced the change of inflammatory cytokines

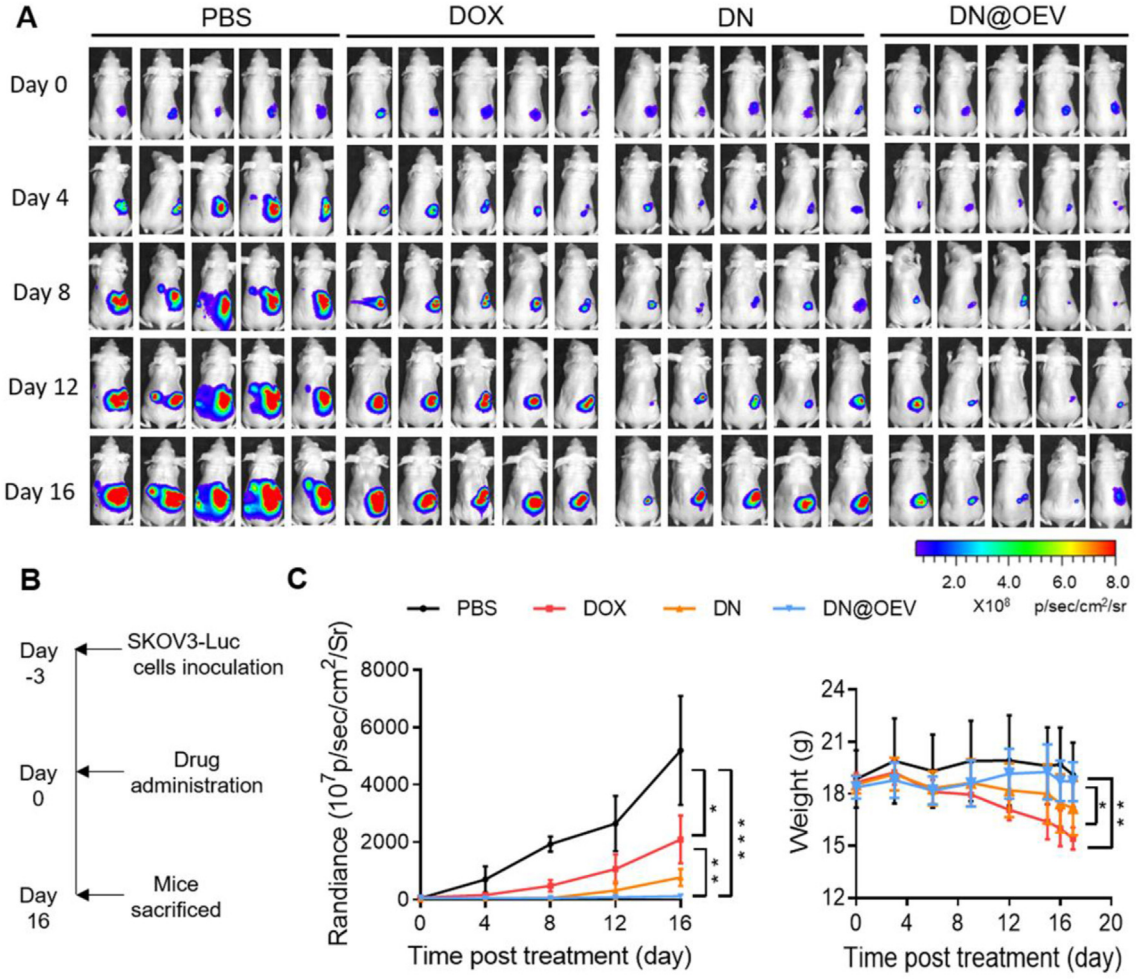

Figure 7 Antitumor efficacy of DN@OEV in orthotopic SKOV3 ovarian cancer xenograft nude mouse. (A) IVIS bioluminescent imaging of orthotopic SKOV3 ovarian cancer xenograft nude mouse from each group during treatment. All mice were injected SKOV3 cells into the ovaries, followed by treatment and measurement of bioluminescence after 3 days (Day 0). The mice were intraperitoneally treated with free DOX, DN or DN@OEV (2.5 mg/kg DOX) every three days using PBS as control group. The tumor size was quantified by IVIS every 4 days. (B) Protocol for tumor treatment of DOX, DN and DN@OEV. (C) The luminescent signal intensity and body weight of the mice in all groups. Results are represented as mean ± SD ($n = 5$). *$P < 0.05$, **$P < 0.01$, and ***$P < 0.001$.

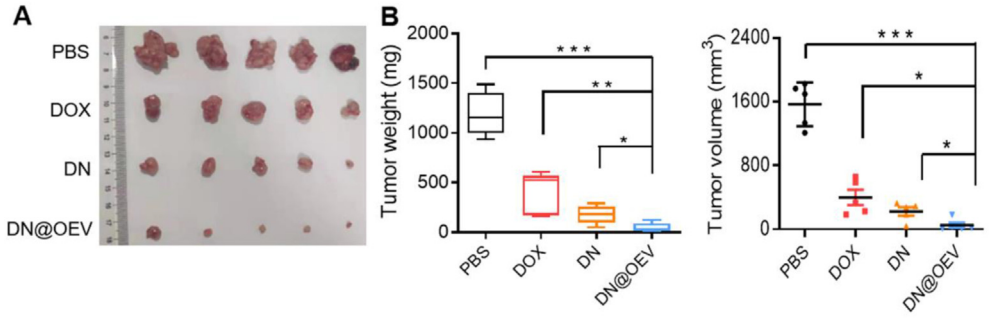

Figure 8 Antitumor efficacy of DN@OEV in orthotopic SKOV3 ovarian cancer xenograft nude mouse. (A) Image of excised tumor of the mouse from each group. (B) Tumor volume and weight of the mice in all groups. Results are represented as mean ± SD ($n = 5$). *$P < 0.05$, **$P < 0.01$, and ***$P < 0.001$.

(IL-1β, IL-6, IP-10, and TNF-α) (Supporting Information Fig. S13). It was shown that chemotherapeutic agent DOX could induce increased proinflammatory cytokines compared with OEV and DN@OEV, indicating OEV presented good biosafety and DN@OEV could not produce strong immunogenicity *via* intraperitoneal injection. To verify the suppression mechanisms, we performed immunohistochemical analysis for Ki67 (a marker for cellular proliferation) and CD34 (a marker for the endothelial-lined vessels) (Fig. 9C). It was shown that the least number of Ki67-positive cells was observed in the tumors treated with DN@OEV, followed by the DN group while there was no obvious difference between PBS and DOX groups, respectively. The results suggest DN@OEV effectively inhibited cell proliferation in ovarian cancer. In addition, the number of tubes consisting of

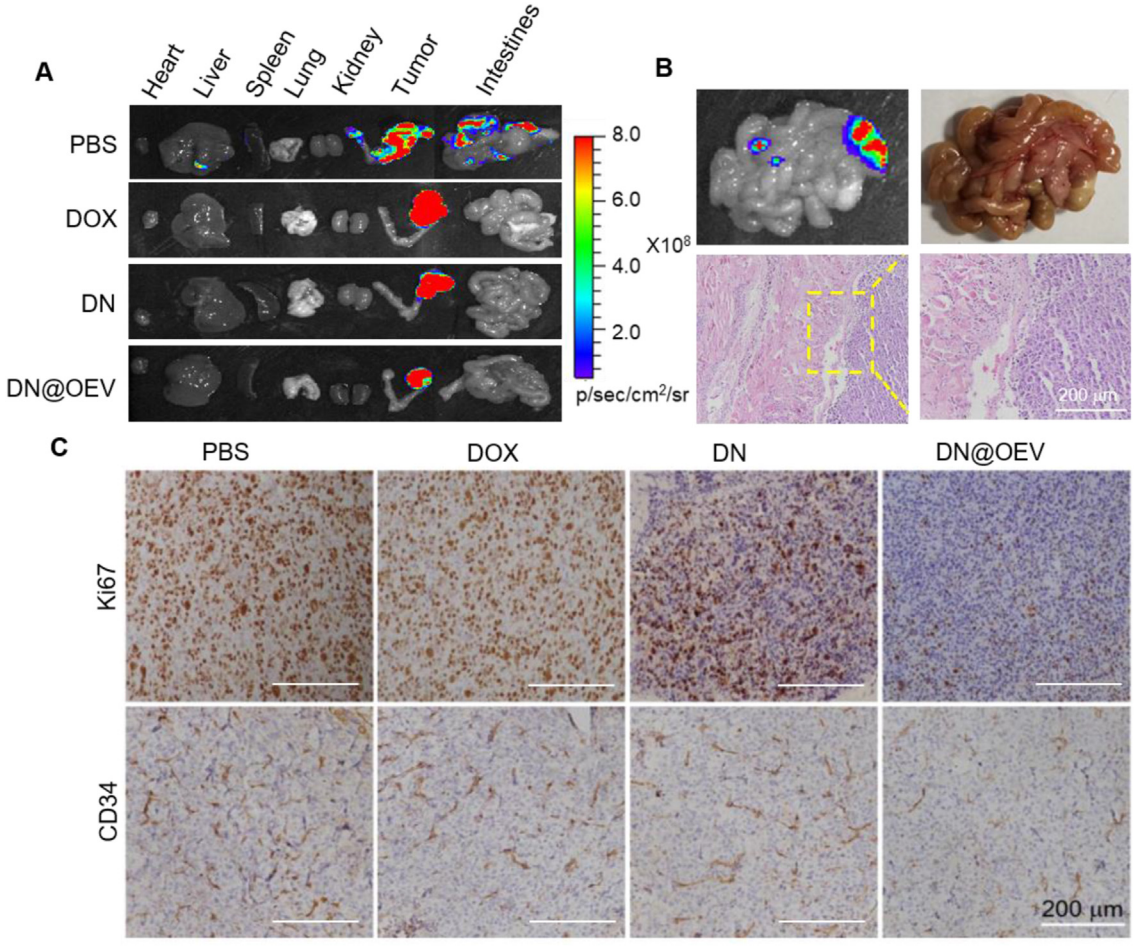

Figure 9 The detection of metastasis after treatment. (A) Photographs and luminescent signal of major organs and tumors of mice in all groups to detect metastasis. (B) Images and HE staining of metastatic nodules of intestines in PBS group. (C) Ovarian cancer tumors of different treatment groups were immunostained with Ki67 for cell proliferation and with CD34 for the detection of endothelial-lined vessels. Scale bar: 200 μm.

$CD34^+$ endothelial-lined vessels in the DN@OEV groups was significantly lower than that of DN, DOX, and PBS, indicating our DN@OEV could efficiently inhibit angiogenesis in ovarian cancer. These results indicate that DN@OEV exhibited a significant capacity to suppress tumor growth and metastasis through anti-proliferation and anti-angiogenesis in ovarian cancer therapy.

4. Conclusions

In this study, we fabricated cRGD-targeted orange-derived extracellular vesicle-based nanodrugs (DN@OEV), enabling the improvement of tumor accumulation and penetration ability, thereby efficiently inhibiting the growth of ovarian cancer. DN@OEV could reduce degradation in the early endosomes-late endosomes−lysosome pathway by receptor-mediated endocytosis and simultaneously promote early endosome/recycling endosomes pathway for exocytosis, resulting in inducing enhanced transcytosis. Thus, active transcytosis would unlock strategies to enhance the delivery efficiency of the drug delivery system in tumor therapy.

Acknowledgments

This work was supported by the National Natural Science Foundation of China (22275080, 22075127, and 82073340) and the Natural Science Foundation of Guangdong Province (2022A 1515012044, China).

Author contributions

Ying Wang and Jun-Bing Fan designed the research. Feng Long, Yao Pan, and Jinheng Li carried out the experiments and performed data analysis. Suinan Sha and Xiubo Shi participated in part of the experiments. Ying Wang and Jun-Bing Fan wrote the manuscript and revised the manuscript. All of the authors have read and approved the final manuscript.

Conflicts of interest

The authors have no conflicts of interest to declare.

Appendix A. Supporting information

Supporting data to this article can be found online at https://doi.org/10.1016/j.apsb.2023.04.006.

References

1. van der Meel R, Sulheim E, Shi Y, Kiessling F, Mulder WJM, Lammers T. Smart cancer nanomedicine. *Nat Nanotechnol* 2019;**14**:1007−17.
2. Parodi A, et al. Bromelain surface modification increases the diffusion of silica nanoparticles in the tumor extracellular matrix. *ACS Nano* 2014;**8**:9874−83.
3. Xu F, Huang X, Wang Y, Zhou S. A size-changeable collagenase-modified nanoscavenger for increasing penetration and retention of nanomedicine in deep tumor tissue. *Adv Mater* 2020;**32**:e1906745.
4. Minchinton AI, Tannock IF. Drug penetration in solid tumours. *Nat Rev Cancer* 2006;**6**:583−92.
5. Heldin CH, Rubin K, Pietras K, Ostman A. High interstitial fluid pressure an obstacle in cancer therapy. *Nat Rev Cancer* 2004;**4**:806−13.
6. Villasenor R, Lampe J, Schwaninger M, Collin L. Intracellular transport and regulation of transcytosis across the blood−brain barrier. *Cell Mol Life Sci* 2019;**76**:1081−92.
7. Bomsel M. Transcytosis of infectious human immunodeficiency virus across a tight human epithelial cell line barrier. *Nat Med* 1997;**3**:42−7.
8. Simister NE, Mostov KE. *Transcytosis Cel* 1985;**43**:389−90.
9. Liu X, Jiang J, Meng H. An effective targeting strategy that is complementary to "EPR effect" for pancreatic cancer nano drug delivery. *Theranostics* 2019;**9**:8018−25.
10. Wang G, et al. Enzyme-triggered transcytosis of dendrimer−drug conjugate for deep penetration into pancreatic tumors. *ACS Nano* 2020;**14**:4890−904.
11. Suzuki H, Bae YH. Evaluation of drug penetration with cationic micelles and their penetration mechanism using an *in vitro* tumor model. *Biomaterials* 2016;**98**:120−30.
12. Liu Y, et al. Transcytosis of nanomedicine fortumor penetration. *Nano Lett* 2019;**19**:8010−20.
13. Sindhwani S, et al. The entry of nanoparticles into solid tumours. *Nat Mater* 2020;**19**:566−75.
14. Pandit S, Dutta D, Nie S. Active transcytosis and new opportunities for cancer nanomedicine. *Nat Mater* 2020;**19**:478−80.
15. Dad HA, Gu TW, Zhu AQ, Huang LQ, Peng LH. Plant exosome-like nanovesicles: emerging therapeutics and drug delivery nanoplatforms. *Mol Ther* 2021;**29**:13−31.
16. Kim J, Li S, Zhang S, Wang J. Plant-derived exosome-like nanoparticles and their therapeutic activities. *Asian J Pharm Sci* 2022;**17**:53−69.
17. Kalluri R, LeBleu VS. The biology, function, and biomedical applications of exosomes. *Science* 2020;**367**:eaau6977.
18. Herrmann IK, Wood MJA, Fuhrmann G. Extracellular vesicles as a next-generation drug delivery platform. *Nat Nanotechnol* 2021;**16**:748−59.
19. Cong M, et al. Technology insight: plant-derived vesicles—how far from the clinical biotherapeutics and therapeutic drug carriers? *Adv Drug Deliv Rev* 2022;**182**:114108.
20. Xiao Q, et al. Lemon-derived extracellular vesicles nanodrugs enable efficiently overcome cancer multidrug resistance by endocytosis-triggered energy dissipation and energy production reduction. *Adv Sci* 2022;**9**:e2105274.
21. Liu S, et al. Extracellular vesicles: emerging tools as therapeutic agent carriers. *Acta Pharm Sin B* 2022;**12**:3822−42.
22. Wang Q, et al. Delivery of therapeutic agents by nanoparticles made of grapefruit-derived lipids. *Nat Commun* 2013;**4**:1867.
23. Zhuang X, et al. Grapefruit-derived nanovectors delivering therapeutic miR17 through an intranasal route inhibit brain tumor progression. *Mol Ther* 2016;**24**:96−105.
24. Niu W, et al. A biomimetic drug delivery system by integrating grapefruit extracellular vesicles and doxorubicin-loaded heparin-based nanoparticles for glioma therapy. *Nano Lett* 2021;**21**:1484−92.
25. Xu G, Liu D, Chen J, Ye X, Ma Y, Shi J. Juice components and antioxidant capacity of citrus varieties cultivated in China. *Food Chem* 2008;**106**:545−51.
26. Xu P, et al. Tumor suppressor TET2 promotes cancer immunity and immunotherapy efficacy. *J Clin Invest* 2019;**129**:4316−31.
27. Ramanathapuram L, Hahn T, Dial S, Akporiaye E. Chemo-immunotherapy of breast cancer using vesiculated alpha-tocopheryl succinate in combination with dendritic cell vaccination. *Nutr Cancer* 2005;**53**:177−93.
28. Lv H, et al. Vitamin C preferentially kills cancer stem cells in hepatocellular carcinoma *via* SVCT-2. *NPJ Precis Oncol* 2018;**2**:1.
29. Ghorbani A, Nazari M, Jeddi-Tehrani M, Zand H. The citrus flavonoid hesperidin induces P53 and inhibits NF-κB activation in order to trigger apoptosis in NALM-6 cells: involvement of PPARγ-dependent mechanism. *Eur J Nutr* 2012;**51**:39−46.
30. Wang L, et al. Enhanced intracellular transcytosis of nanoparticles by degrading extracellular matrix for deep tissue radiotherapy of pancreatic adenocarcinoma. *Nano Lett* 2019;**22**:6877−87.

31. Stanly C, Moubarak M, Fiume I, Turiák L, Pocsfalvi G. Membrane transporters in *Citrus clementina* fruit juice-derived nanovesicles. *Int J Mol Sci* 2019;**20**:6205.
32. Patel MM, Patel BM. Crossing the blood−brain barrier: recent advances in drug delivery to the brain. *CNS Drugs* 2017;**31**:109−33.
33. Tajes M, et al. The blood−brain barrier: structure, function and therapeutic approaches to cross it. *Mol Membr Biol* 2014;**31**: 152−67.
34. Sahay G, Alakhova DY, Kabanov AV. Endocytosis of nanomedicines. *J Control Release* 2010;**145**:182−95.
35. Kornilova ES. Receptor-mediated endocytosis and cytoskeleton. *Biochemistry (Mosc)* 2014;**79**:865−78.
36. Grant BD, Donaldson JG. Pathways and mechanisms of endocytic recycling. *Nat Rev* 2009;**10**:597−608.
37. Maxfield FR, McGraw TE. Endocytic recycling. *Nat Rev* 2004;**5**:121−32.
38. Harisa GI, Badran MM, Alanazi FK, Attia SM. An overview of nanosomes delivery mechanisms: trafficking, orders, barriers and cellular effects. *Artif Cells, Nanomed Biotechnol* 2018;**46**:669−79.
39. Teng F, Fussenegger M. Shedding light on extracellular vesicle biogenesis and bioengineering. *Adv Sci* 2021;**8**:2003505.
40. van Niel G, Angelo GD, Raposo G. Shedding light on the cell biology of extracellular vesicles. *Nat Rev* 2018;**19**:213−28.
41. Prabaharan M, Grailer JJ, Pilla S, Steeber DA, Gong S. Amphiphilic multi-arm-block copolymer conjugated with doxorubicin *via* pH-sensitive hydrazone bond for tumor-targeted drug delivery. *Biomaterials* 2009;**30**:5757−66.
42. Stenmark H. Rab GTPases as coordinators of vesicle traffic. *Nat Rev Mol Cell Biol* 2009;**10**:513−25.